CFD simulations of the flow around a bottom-fixed vertical pile with a n-Euler approach

Gaétan Pierre[1,2], William Benguigui[1,3], Jérôme Laviéville[1], Pascal Fede[2] and Olivier Simonin[2]

[1]EDF R&D, Fluid Mechanics Division, 6 quai Watier, Chatou, FR-78400, France
[2]Institut de Mécanique des Fluides de Toulouse (IMFT), Université de Toulouse, CNRS, Toulouse, FR-31400, France
[3]IMSIA, UMR EDF-ENSTA-CNRS-CEA 9219, Paris-Saclay University, Palaiseau, FR-91762, France
Corresponding author: gaetan.pierre@edf.fr.

ABSTRACT

The simulation of the free surface flow around a circular pile over a rigid bed is carried out with a Eulerian-Eulerian approach where a mass and momentum transport equations are solved for both phases. A wall-resolved second-order turbulence model is used. The velocity field and the bed shear stress around the pile are found to be in correct agreement with experimental data. Taking into account the free surface does not modify significantly the flow for a Froude number of 0.14. The coherent structures of the horseshoe vortex system are described. A bottom-attached vortex rotating clockwise and located at the bottom of the primary horseshoe vortex is present in the time-averaged flow field.

INTRODUCTION

The flow around a bottom-fixed pile exhibits complex features. The streamlines contract at the sides of the pile, lee-wake vortices are generated downstream, and the so-called horseshoe vortex system is present, if the operating conditions allow it, close to the bed, upstream the pile and extent to its sides. Those flow features locally increase the bed shear stress around the pile. When the bed is deformable, such as the seabed composed of sediments, additional sediment transport, known as local scour, happens over time and a hole about the size of the pile diameter is formed. The understanding of local scour around a pile is of primary interest in the offshore wind industry in order to prevent wind turbine foundations from being exposed, threatening their stability.

Extensive research on local scour have been carried in the literature, both experimentally and more recently with numerical simulations. A focus on the flow and local scour around a circular pile is made since by the end of 2020, 81.2% of installed offshore wind turbine in Europe had a monopile (circular pile) substructure (Ramirez 2020).

Dargahi (1990) studied the scouring process under steady current around a circular pile for pile Reynolds number of $Re_D = 20{,}000$ and $Re_D = 39{,}000$. The author gave an extensive description of the horseshoe vortex system during the scouring process. During the initial stage, which is on a flat bed, the author observed i) two primary clockwise rotating vortices (PV1 and PV2), ii) two smaller bottom-attached counterclockwise rotating vortices (BAV1 and BAV2) confined between the bed and the primary vortices and iii) a counterclockwise rotating vortex (JV) at the junction of the pile and the bed. The primary vortices moved back and forth over time. This bimodal unsteadiness of the horseshoe vortex system was first reported by Devenport and Simpson (1990). The bottom-attached vortices were not permanent. More recently, other researchers have reported only one (Jenssen 2019) or two (Apsilidis *et al.* 2016) primary vortices, no bottom-attached vortices and a junction vortex from time-averaged flow field measurements.

Roulund *et al.* (2005) studied the flow over a flat rigid bed and the scouring process around a bottom-fixed circular pile exposed to steady current both experimentally and numerically. The maximum bed shear stress amplification was located at a 45° to 70° angle from the flow direction. The numerical model was based on the Reynolds-averaged Navier-Stokes equations for the hydrodynamic model and on the mesh moving (Arbitrary Lagrangian Eulerian method) approach to compute the bed deformation when scouring was considered. The turbulent closure model was the $k - \omega$ SST model. The free surface was not taken into account like most numerical studies on local scour in the literature.

Nagel *et al.* (2020) simulated the rigid-bed Test 1 and the scouring Test 3 of Roulund *et al.* (2005). The author used the Euler-Euler approach where a mass and a momentum balance equation are solved for each phase (water and sediment). The free surface was not taken into account. To our knowledge, this was the first 3D scouring simulation with this kind of approach. Satisfactory agreement was found with experimental data.

In the present work, the simulation of the flow around a vertical cylinder fixed onto a flat and rigid bed and exposed to steady current is carried out. First, the governing equations of the multi-Eulerian approach are introduced. Then the numerical model is presented, results are discussed and finally conclusion and perspectives are drawn.

NUMERICAL MODELING

Governing Equations

The 3D numerical simulations are carried out with the neptune_cfd code. This finite-volume Eulerian n-fluid unstructured parallelized multiphase flow software is developed in the framework of the NEPTUNE project financially supported by EDF (Electricité De France, CEA (Commisariat à l'Energie Atomique), IRSN (Institut de Radioprotection et de Sureté Nucléaire) and Framatome.

The transport equations for mass, momentum and energy are derived by phase ensemble averaging and are solved for each phase and coupled through inter-phase transfer terms. The mass transport equation is written

$$\frac{\partial}{\partial t}(\alpha_k \rho_k) + \frac{\partial}{\partial x_j}\left(\alpha_k \rho_k u_{k,j}\right) = 0 \tag{1}$$

where α_k is the volume fraction, ρ_k the density and $u_{k,j}$ the mean velocity j^{th} component of the phase k.

The i-th component of the mean momentum transport equation is written

$$\frac{\partial}{\partial t}\left(\alpha_k \rho_k u_{k,i}\right) + \frac{\partial}{\partial x_j}\left(\alpha_k \rho_k u_{k,i} u_{k,j}\right) =$$

$$-\alpha_k \frac{\partial p}{\partial x_i} + \alpha_k \rho_k g_i + \frac{\partial}{\partial x_j}\left(\alpha_k \Sigma_{k,ij} - \alpha_k \rho_k R_{k,ij}\right) + \sum_{q \neq k} I_{(q->k),i} \tag{2}$$

where p is the mean pressure, g_i is the gravitational acceleration, $R_{k,ij}$ the Reynolds stress tensor, $I_{(q->k),i}$ the interfacial momentum transfer term from phase q to phase k (for example friction between air and water for free surface flows) and $\Sigma_{k,ij} = 2\mu_k S^D_{k,ij}$ the viscous stress tensor where μ_k is the dynamic viscosity and $S^D_{k,ij}$ the deviatoric strain-rate tensor

$$S^D_{k,ij} = \frac{1}{2}\left(\frac{\partial u_{k,i}}{\partial x_j} + \frac{\partial u_{k,j}}{\partial x_i}\right) - \frac{1}{3}\frac{\partial u_{k,l}}{\partial x_l}\delta_{ij} \tag{3}$$

Turbulence modeling

The Reynolds stress tensor is closed with the $R_{ij} - \epsilon$ EBRSM model (Elliptic Blending Reynolds-Stress Model) (Manceau and Hanjalic 2002) where a transport equation for each Reynolds stress tensor components $R_{k,ij} = \langle u'_{k,i} u'_{k,j} \rangle$ and for the turbulent kinetic energy dissipation ϵ_k is solved.

Momentum transfer for free surface flows

The gas-liquid interface tracking and its interfacial momentum transfer $I_{(q->k),i}$ from friction is modeled by the Large Interface Model (Coste 2013).

Test case operating conditions

In the present work, the simulation of Roulund *et al.* (2005) experiment (Test 1) of a bottom-fixed circular pile exposed to steady current in an open channel over a rigid, flat and hydrodynamically smooth bed have been carried out. The pile diameter is $D = 0.536$ m, the water depth is $H = 0.54$ m and the bulk velocity is $u_{ref} = 0.326$ m/s which yields a pile Reynolds number of $Re_D = 1.7 \times 10^5$ and a Froude number of $Fr = 0.14$.

Initial and boundary conditions

Figure 1 shows the simulation domain and the boundary condition associated with each boundary zone.

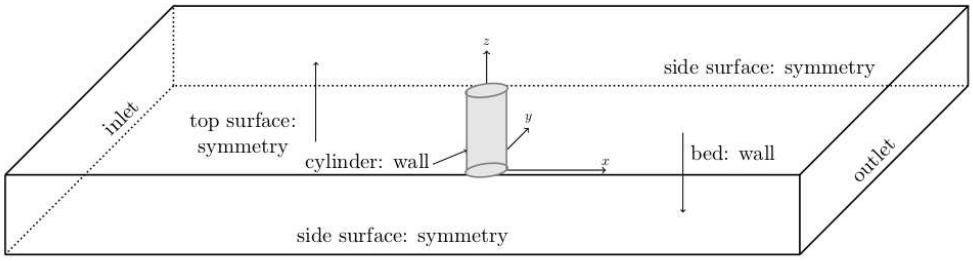

Figure 1. Sketch of the simulated domain and boundary conditions of each boundary surfaces.

The velocity is initially set at zero and the pressure is set to the atmospheric pressure in all the domain. For free surface simulations, a cell-center is located exactly at the targeted water depth and the volume fraction is set as 0.5 for both phases in that cell.

Bed shear stress

The friction velocity is computed from the van Driest profile

$$\frac{u_\tau}{u_*} = 2\int_0^{y_I{}^+} \frac{\mathrm{d}y^+}{1+\sqrt{1+4\kappa^2 y^{+2}[1-\exp(-y^+/A)]}} \tag{7}$$

where u_τ is the tangential velocity (in the referential of the boundary face), u_* the friction velocity, $y_I{}^+ = y_I u_*/\nu$ and y_I is the distance from the face center to the cell center I, κ the von Karman constant and A the van Driest damping factor set at 0.42 and 25.6 respectively. The right-hand side of Eq. (7) is approximated by a 10th-order polynomial as a function of yu_τ/ν. Then, the bed shear stress is computed as

$$\tau_0 = \rho u_*^2 \times sign(u_x) \tag{8}$$

The bed shear stress amplification is obtained by dividing the bed shear stress with the undisturbed bed shear stress $\tau_\infty = \rho u_{*,\infty}^2$ where $u_{*,\infty} = 0.013$ m/s following Roulund *et al.* (2005).

Computational mesh

The simulation domain length, width and height are respectively $20D$, $10D$ and 1D where the cylinder diameter is $D = 0.536$ m. Figure 2 shows a view of the computational mesh used in the present work. The mesh is refined around the pile to capture the horseshoe vortices and downstream to capture the lee-wake vortices. A mesh sensitivity analysis was carried (not shown here) and the final mesh have 256 cells around the cylinder perimeter, 64 and 96 cells across the water depth for the rigid-lid and the free surface simulations respectively. In total, the meshes are made of 3.506 million and 5.259 million hexahedral cells. The smallest cell size is $\Delta y = 0.13$ mm and is located at the bed and around the cylinder in order to verify $y^+ = yu_f/\nu < 1$ at all times.

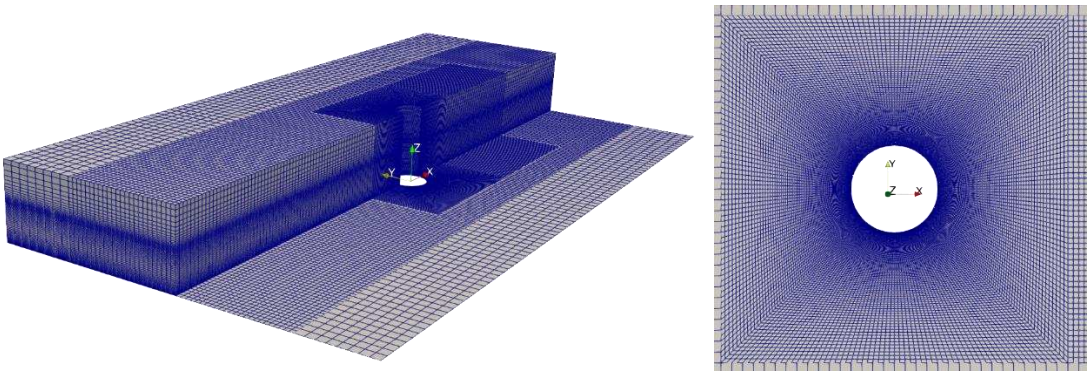

Figure 2. Full mesh of the free surface simulation and zoom around the pile.

RESULTS

Figure 3 shows the time-averaged velocity magnitude and the time-averaged streamlines in the *xz*-plane along the symmetry, in front of the cylinder and zoomed in close to the bed. The time averaging procedure was started after 20 lee-wake vortex shedding vortex period (~ 100 s) and lasted 40 period (~ 200 s). From this figure, we can see the downflow close to the cylinder which create a horizontal jet towards the upstream direction at the bed level. A large clockwise rotating vortex (PV1) is located at x/D = -0.805 and z/D = 0.054 and expand from x/D = -0.9 to x/D = -0.7 and from z/D = 0.005 to z/D = 0.010 (=53.6 mm). We also notice a counterclockwise rotating vortex at the junction between the bed and the pile (JV) which center is located at x/D = -0.505 and z/D = 0.012. Finally, we see a small, bottom attached, counterclockwise rotating vortex upstream PV1 (BAV1) which center is located at x/D = -0.884 and z/D = 0.003 and expand from x/D = -0.890 to x/D = -0.870. Bottom-attached vortex have been reported in previous experimental study (Dargahi 1999; Qi *et al.* 2022) and LES simulations (Kirkil *et al.* 2008; Zhang *et al.* 2020) of such flow. This vortex is not coherent in time and may be filtered by a time-averaging procedure. We suppose that we captured this BAV1 vortex thanks to a fine mesh close to the bed and to our second-order turbulence closure model $R_{ij} - \varepsilon\, EBRSM$. Finally, the size of the horseshoe vortex system is $x_s/D = 0.9$, in agreement with Roulund *et al.* (2005).

Figure 4 shows the longitudinal and vertical velocity profile along the longitudinal axis upstream and downstream the cylinder at different heights. The main features of the flow around a bottom-fixed cylinder can be observed from those profiles: a downflow upstream the cylinder and above z = 50 mm, a clockwise rotating vortex between x/D = -0.9 and x/D = -0.7 and under z = 50 mm and a counter-clockwise rotating vortex against the cylinder and under z = 10 mm. Overall, we can see that our numerical results (blue line) agree well with Roulund *et al.* (2005) experimental data (black dots). There is a discrepancy in the vertical velocity downstream and close to the cylinder at z=200 mm, z=100 mm and z=50 mm. This discrepancy with the experimental results was also reported by Zhou (2017) and Nagel *et al.* (2020). We found that a free surface simulation does not reduce this discrepancy significantly (not shown here), in agreement with Zhou (2017) conclusion.

Figure 5 shows the time-averaged bed shear stress amplification in the *xy*-plane around the cylinder. We can see that the maximum amplification is located between 50° and 82° angle with the x-axis on both sides and very close to the cylinder. This is due to the contraction of the streamlines. We also notice an amplification of about 3 upstream the cylinder at around x/D = -0.8 which is due to the primary horseshoe vortex PV1. This vortex is stretched by the flow on both sides of the cylinder and extend downstream the cylinder.

Figure 6 shows the time-averaged bed shear stress amplification along the x-axis upstream the cylinder. We underestimate the amplification by 20% upstream far from the cylinder. Between x/D = -0.93 and x/D=-0.85, the bed shear stress amplification becomes positive because of the presence of the counterclockwise rotating vortex BAV1. Other authors (Roulund *et al.* 2005; Baykal *et al.* 2015, Nagel *et al.* 2020) have not reported this vortex. Since they are no experimental data of the bed shear stress in this region, we cannot conclude if this vortex did exist or not in the experiment. Then from x/D = -0.85 to x/D = -0.7, the vortex PV1 induce a large negative bed shear stress amplification. Our simulation results are twice greater than experimental data. No explanation can be provided to explain such large discrepancy. We suppose that the $R_{ij} - \varepsilon\, EBRSM$ turbulence model used in the present work is responsible for the discrepancy with other authors results where different versions of the $k - \omega$ turbulence model was used. From x/D=-0.7 to x/D=-0.52, the negative bed shear stress is caused by the horizontal jet and our numerical results match experimental data well. Finally, from x/D=-0.52 to x/D=-0.50, we see a positive bed shear stress amplification because of the presence of the counterclockwise rotating junction vortex JV. The maximum value of 0.6 obtained in this region is twice larger than reported by Roulund *et al.* (2005) and Nagel *et al.* (2020). There is no experimental data of the bed shear stress close to the cylinder to compare with. On a similar experiment with slightly different operating conditions ($Re_D = 39{,}000$ and $Fr = 0.32$) from Jenssen (2019) we found a similar maximum bed shear stress amplification of 0.5 in the junction vortex region, in agreement with Jenssen (2019) experimental data.

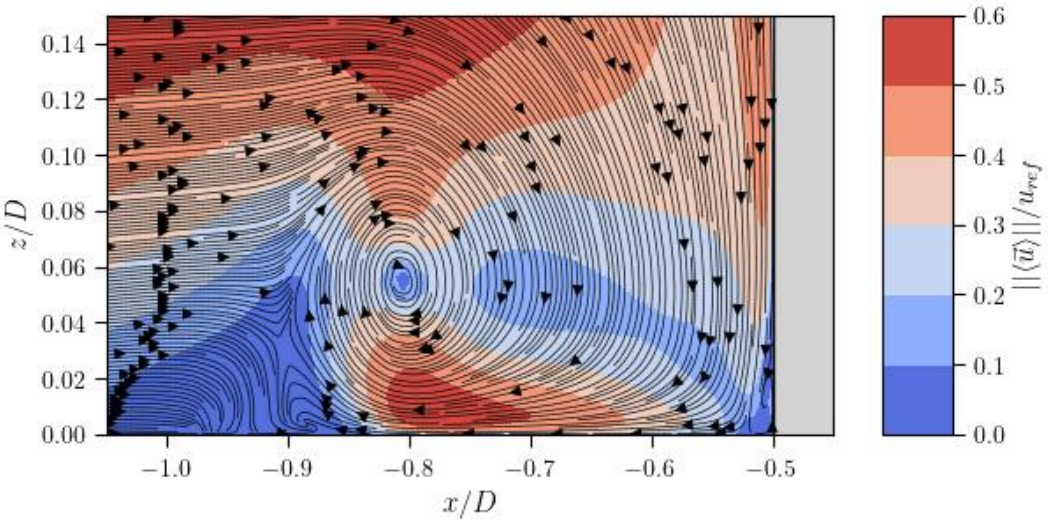

Figure 3. Dimensionless magnitude of the time-averaged velocity and streamlines in front of the cylinder.

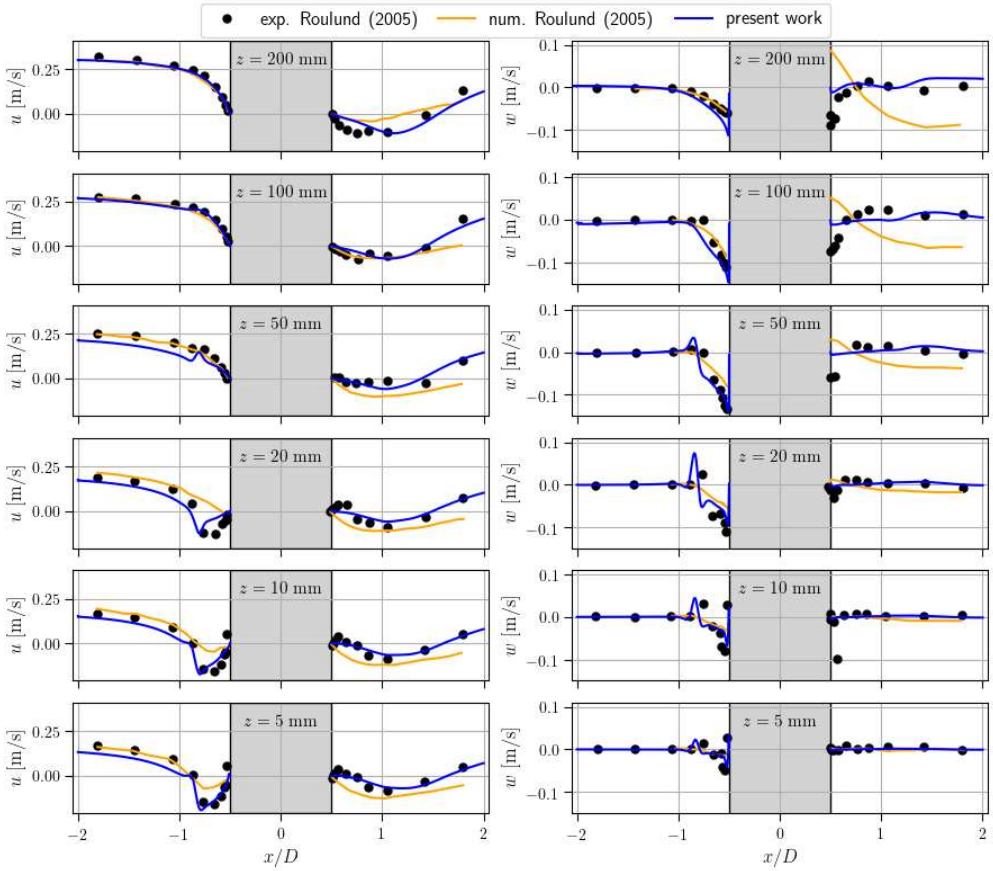

Figure 4. Longitudinal velocity (left) and vertical velocity (right) along the longitudinal axis upstream and downstream of the cylinder at different heigh

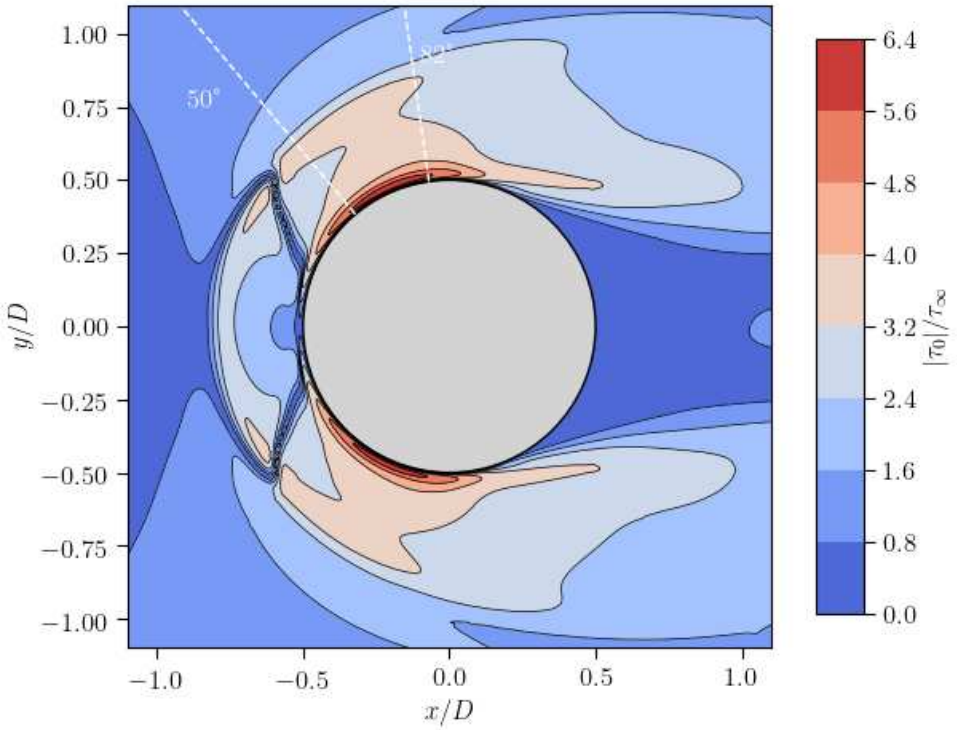

Figure 5. Time-averaged magnitude of the bed shear stress amplification around the cylinder.

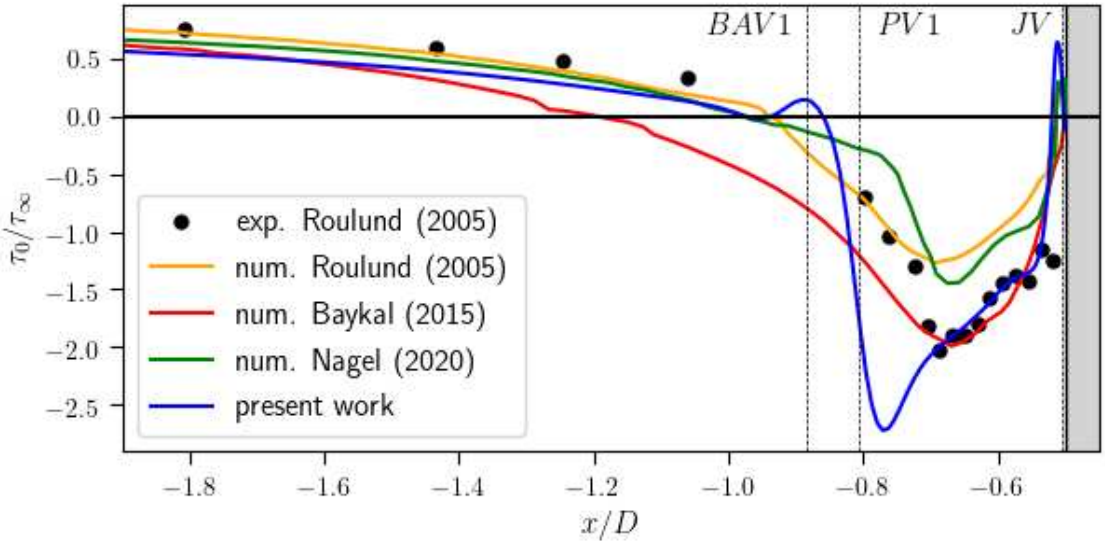

Figure 6. Time-averaged bed shear stress amplification along the longitudinal axis upstream the cylinder.

CONCLUSION

The simulation of the flow around a circular pile fixed to a rigid and flat bed and exposed to a steady current have been carried out with a multi-Eulerian approach and a second order wall resolved $R_{ij} - \varepsilon$ turbulence model. The horseshoe vortex system obtained has been discussed extensively. Overall, we obtained good agreement with experimental results. We note that we captured a small, counterclockwise bottom-attached vortex next to the primary horseshoe vortex. This vortex has been reported in experimental studies and LES simulations but is not time-coherent and is often filtered after a time averaging procedure. Nevertheless, a turbulence model sensitivity analysis will be conducted to confirm if the presence of this vortex is due to the second order $R_{ij} - \varepsilon\, EBRSM$ turbulence model used in the present work. The validation of the neptune_cfd code to simulate the flow around a vertical pile will be continued by exposing the pile to waves (Sumer *et al.* 1997). The waves will be produced with a numerical wave tank (free surface) and with an oscillatory flow (no free surface). Then, the rigid bed will be replaced by sediments modeled as a Eulerian phase. Eulerian particulate phase models are already implemented in neptune_cfd and have been validated on many fluid-particles applications ranging from dilute to dense regimes (Fede *et al.* 2016; Bennani *et al.* 2017; Hamidouche *et al.* 2019; Neau *et al.* 2020; Audard *et al.* 2021). Scouring simulations of a circular pile exposed to a steady current (Roulund *et al.* 2005) or waves (Sumer *et al.* 1992) will be carried out. Finally, more complex geometries than a circular pile such as a jacket could be considered by using the Immersed Boundary Method (Benguigui *et al.* 2018) already implemented in neptune_cfd.

REFERENCES

Apsilidis, N., P. Diplas, C. L. Dancey, P. Bouratsis. 2016. “Effects of wall roughness on turbulent junction flow characteristics”. *Exp. Fluids.* 57 (12), 1–12.

Audard, F., P. Fede, E. Belut, J. R. Fontaine, H. Neau, O. Simonin. 2021. “Eulerian modelling of the powder discharge of a silo: Attempting to shed some light on the origin of jet expansion”. *Powder Technol.* 379, 49–57.

Baykal, C., B. M. Sumer, D. R. Fuhrman, N. G. Jacobsen, J. Fredsøe. 2015. “Numerical investigation of flow and scour around a vertical circular cylinder”. *Phil. Trans. R. Soc.* A 373: 20140104.

Bennani, L., H. Neau, C. Baudry, J. Laviéville, P. Fede, O. Simonin. 2017. “Numerical simulation of unsteady dense granular flows with rotating geometries”. Chem. Eng. Res. Des. 120, 333–347.

Benguigui, W., A. Doradoux, J. Lavieville, S. Mimouni, E. Longatte. 2018. “A discrete forcing method dedicated to moving bodies in two-phase flow”. *Int. J. Numer. Meth. Fluids.* 1–19.

Coste, P. 2013. “Large Interface Model for two-phase CFD”. *Nucl. Eng. Des.* 255, 38–50.

Dargahi, B. 1990. “Controlling Mechanism of Local Scouring”. *J. Hydraul. Eng.* 116 (10), 1197–1214

Devenport, W. J., and R. L. Simpson. 1990. “Time-dependent and time-averaged turbulence structure near the nose of a wing–body junction”. *J. Fluid Mech*. 210, 23–55.

Fede, P., O. Simonin, A. Ingram. 2016. “3D numerical simulation of lab-scale pressurized dense fluidized bed reactor focussing on the effect of the particle-particle restitution coefficient and particle-wall boundary conditions”. *Chem. Eng. Sci.* 142, 215–235.

Hamidouche, Z., E. Masi, P. Fede, O. Simonin, K. Mayer, S. Penthor. 2019. “Unsteady three-dimensional theorical model and numerical simulation of a 120 kW chemical looping combustion pilot plan”. *Chem. Eng. Sci.* 193, 102–119

Jenssen, U. 2019. “Experimental Study of the Flow Field Around a Scouring Bridge Pier”. PhD Thesis. Technischen Universität München.

Kirkil, G., S. G. Constantinescu, R. Ettema. 2008. “Coherent Structure in the Flow Field around a Circular Cylinder with Scour Hole”. *J. Hydraul. Eng.* 134 (5), 572–587

Manceau, R., K. Hanjalic. 2002. “Elliptic blending model: a new near-wall Reynolds-stress turbulence closure”. *Phys. Fluids* 14.

Nagel, T., J. Chauchat, C. Bonamy, X. Liu, Zhen Cheng, Tian-Jian Hsu. 2020. “Three-dimensional scour simulations with a two-phase flow model”. *Adv. Water Resour.* 138.

Neau, H., M. Pigou, P. Fede, R. Ansart, C. Baudry, N. Mérigoux, J. Laviéville, Y. Fournier, N. Renon, O. Simonin, 2020. “Massively parallel numerical simulation using up to 36,000 CPU cores of an industrial-scale polydispersed reactive pressurized fluidized bed with a mesh of one billion cells”. *Powder Technol.* 366, 906-924.

Qi, W. G., J. Liu, F. P. Gao, B. Li, Q. G. Chen, 2022. "Quantifying the spatiotemporal evolution of the turbulent horseshoe vortex in front of a vertical cylinder", *Phys. Fluids* 34, 015110.

Roulund, A., B. M. Sumer, J. Fredsøe and J. Michelsen. 2005. “Numerical and experimental investigation of flow and scour around a circular pile.” *J. Fluid Mech*. 534, 351–401.

Sumer, B., N. Christiansen. 1992. “Scour Around Vertical Pile in Waves”. *J. Waterw. Port Coast. Ocean Eng.* 118 (15).

Sumer, B. M., N. Christiansen and J. Fredsøe. 1997. “The horseshoe vortex and vortex shedding around a vertical wall-mounted cylinder exposed to waves.” *J. Fluid Mech*. 332, 41–70.

Ramirez, L., D. Fraile, G. Brindley. 2020. “Offshore wind in Europe – key trends and statistics 2020”. Technical report. Wind Europe.

Zhang W., M. U. Zapata, X. Bai, D. Pham-Van-Bang, K. D. Nguyen. 2020. “Three-dimensional simulation of horseshoe vortex and local scour around a vertical cylinder using an unstructured finite-volume technique.” *Int. J. Sediment Res*, 35 (3) 295-306.